PAPER

Check for updates

IoT-based triboelectric nanogenerator for wrist pulse acquisition and analysis

Karthikeyan V. and Vivekanandan S. [ID] *

Wrist pulse plays a critical role in prediction and diagnosis of blood pressure (BP)-related illnesses. Therefore, a low-cost, noninvasive and cuffless BP measurement is highly anticipated. Hence, this study reports a triboelectric nanogenerator to harvest *nadi* signals for BP measurement. To harvest *nadi* such as *vata*, *pitta* and *kapha*, the triboelectric nanogenerator is designed and placed on a human wrist; notably, the *vata nadi* is prone to hypertension. Herein, time domain and frequency domain analyses are performed to identify *nadi* pulse parameters, which are helpful to monitor the health of subjects. Moreover, an age-wise frequency range of *vata*, *pitta* and *kapha* for male and female individuals are tabulated. The designed triboelectric nanogenerator offers high sensitivity of 0.41 kPa^{-1} in the pressure range of 0.01–3 kPa with an ultrafast response time of <3 ms, and no performance degradation is observed after up to 40 000 motion cycles. Thus, the self-powered capability of the triboelectric nanogenerator ensures reliable health care monitoring of parameters such as the heart rate, glucose range, gait and CO$_2$ levels.

Introduction

Wearable sensors' efficient biomechanical energy gathering capabilities have made them the backbone of health monitoring systems,[1] and the same capabilities are also found in triboelectric nanogenerators (TENGs), which transfer mechanical energy in conjunction with triboelectrification and electrostatic induction.[1] Hence, researchers started focusing on triboelectric nanogenerators to harvest the existing biomechanical energy of the human body at different locations such as the wrist and waist.[2] TENGs are far more superior than other wearable sensors in that they are self-powered, lightweight, inexpensive, reusable, and produced on a large scale.[3] By choosing highly charged opposite tribolayers and introducing some nanostructures on these tribolayers' surfaces, the performance of TENGs can be improved.[4,5] According to Ayurveda, the human health status depends on three Ayurveda *doshas*, namely, *vata*, *pitta* and *kapha*, which are called *tridoshas*; any imbalance in *tridoshas* causes symptoms of diseases. Herein, a TENG is used to acquire the three *nadi* signals by placing it on appropriate *nadi* signal locations, as shown in Fig. 1.

Vata, the most fundamental of the three *doshas*, is composed of space and air. The human body's *vata dosha* is the most significant since it regulates the activities of the other two *doshas*, tissues, and waste products. Essentially, *vata* governs all bodily metabolisms as well as all mental and physical functions. *Vata* facilitates the flow of all sensory signals from various sense

organs to the brain. Additionally, it controls the removal of all biological waste, including sperm, feces, urine, and sweat. *Pitta* is a synthesis of the fire and water components that emerges during the transformation of these combined elements. It controls several processes, such as the metabolism and digestion of food. In addition to overseeing vision, hunger, and skin tone, *pitta* oversees thermogenesis. Bravery and courage are principally the domains of *pitta*. Earth and water form the element of *kapha*. It offers strength to accomplish a variety of physical tasks, stability to give the body and mind the necessary basis, as well as moisture and lubrication to lessen excessive friction in the human body. It oversees vitality and fertility to produce healthy offspring. Each of the three pulses has unique characteristics. The movement of the *vata* pulse is irregular and thin, such as that of a snake. The *pitta* pulse is vivacious and hops around, much like a frog. The *kapha* pulse is powerful, like the gliding of a swan.[6] For pulse diagnosis, data analysis is very

Fig. 1 Illustration of the *vata*, *pitta* and *kapha nadi* positions.

School of Electrical Engineering, Vellore Institute of Technology, Vellore, Tamil Nadu – 632 014, India. E-mail: svivekanandan@vit.ac.in
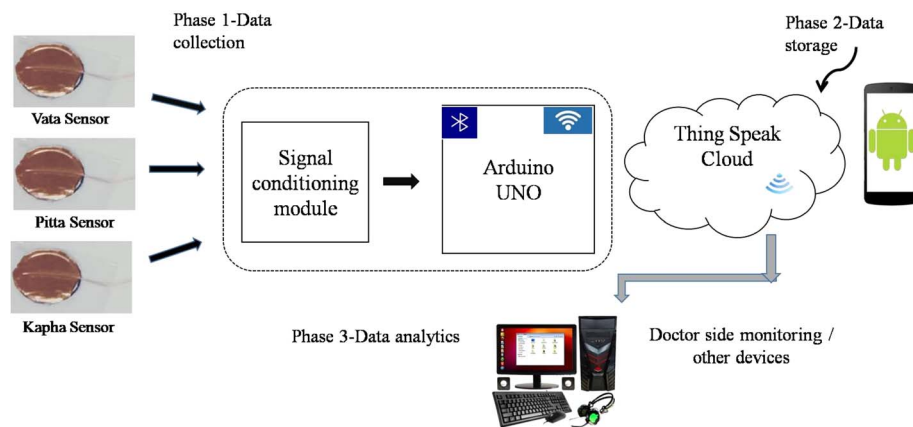
Fig. 2 Hardware block diagram.

crucial. In general, data analysis in the frequency domain retrieves the frequency information underlying the pulses, whereas data analysis in the time domain looks at the geometric shapes of the pulses. Some studies have been conducted on time domain and frequency domain analysis of wrist pulse signal; they are listed below. Dong-Yu Zhang *et al.* in 2010 utilized a doppler ultrasound device to gather blood flow data from the radial artery in the wrist, which was subsequently denoised using an empirical mode decomposition (EMD)-based technique. In the feature extraction module, the extraction of spatial characteristics was preceded by the extraction of spectrum features using a method based on the Hilbert–Huang transform (HHT). Ultimately, in the classification module, patients with two common visceral diseases, cholecystitis and nephritis, were separated from healthy individuals using a support vector machine (SVM) classifier.[7] In 2018, Hung Chang *et al.* introduced the fast Fourier transform to analyze the frequency domain parameters of the acquired wrist pulse
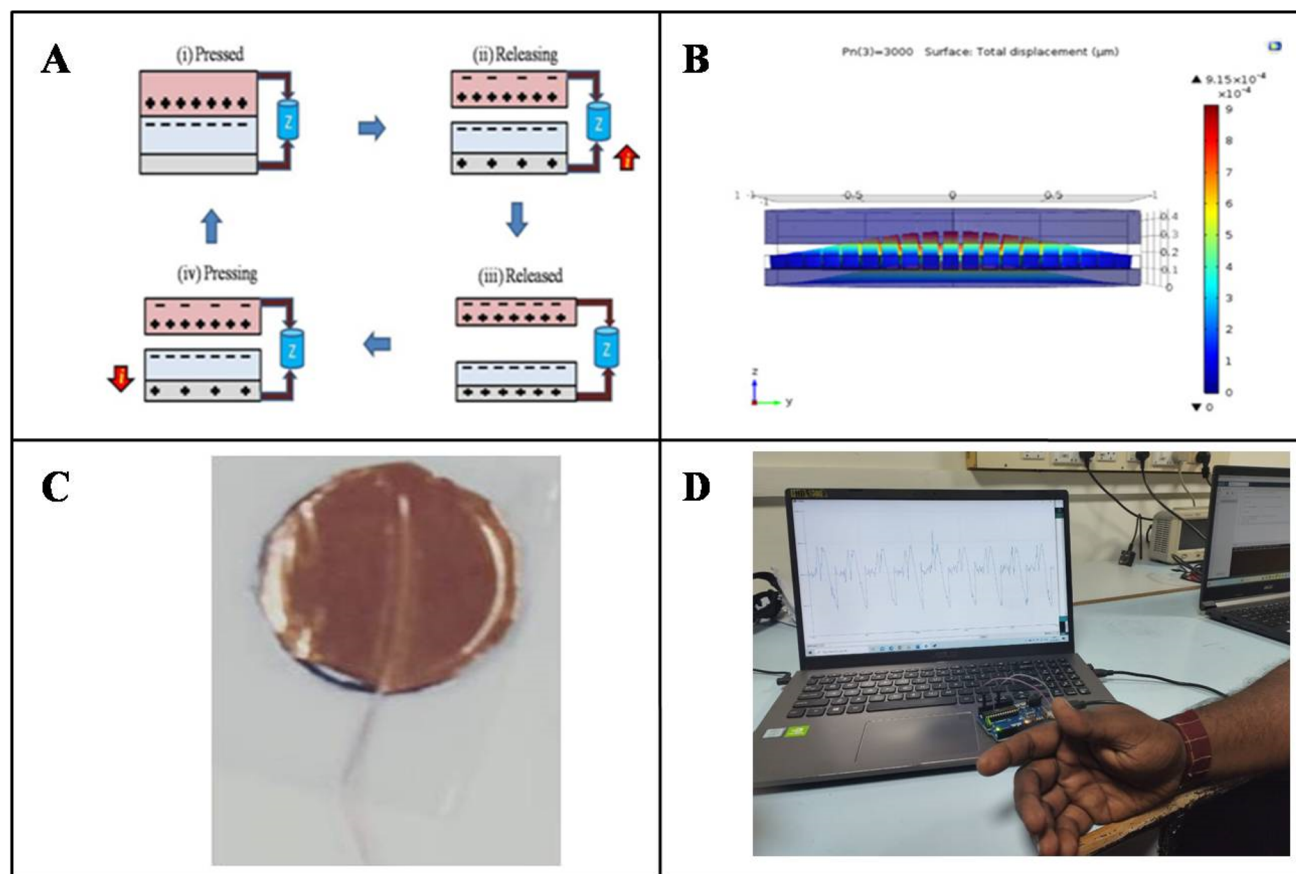

Fig. 3 (A) Operating mechanism of the triboelectric nanogenerator (TENG). (B) COMSOL simulated model of the TENG. (C) Designed TENG. (D) *Nadi* signal acquisition by the designed TENG.

Table 1 Comparison of sensing performance of the material used in this work with other related works

Materials	Sensing mechanism	Sensitivity	Sensing range	Ref.
CCGF	Piezoresistive	0.36 kPa^{-1}	0–2 kPa	16
		4.60% kPa^{-1}	2–5 kPa	
Graphene/Ag	Piezoresistive	1.6% kPa^{-1}	0–40 kPa	17
p-GNP-SR	Piezoresistive	8.65% kPa^{-1}	0–12 kPa	18
Two single-layer graphene	Piezoresistive	-0.24 kPa^{-1}	0.25–0.7 kPa	—
		3.9% kPa^{-1}	1–8 kPa	
ITO-graphene FET-PDMS	Piezoelectric	0.94% kPa^{-1}	0–1.4 kPa	19
MXene/PVDF-TrFE	Capacitive	0.51 kPa^{-1}	0–1 kPa	20
		1.10% kPa^{-1}	1–167 kPa	
PTFE-copper	Triboelectric nanogenerator	41% kPa^{-1}	0.01–3 kPa	Proposed work

signal. The factors that affected the pulse were evaluated through simulations. These factors included vessel stiffness, which changed the pulse's harmonic frequencies, phase shifts of reflected pulse waves, which produced sub-peaks in the pulses, and wave amplitudes, which were based on the pulse strength.[8] Yim *et al.* in 2014 evaluated the variations in depth, total and relative pulse force, breadth, and rhythm at three locations among healthy male and female individuals. They stated that the pulse force of men was greater than that of women. In addition, they noticed that the mean systolic blood pressure (SBP) and diastolic BP were substantially lower in women than in males as well as that the mean SBP was considerably greater in the right wrist than the left wrist in both men and women.[9] In this study, the wrist pulse signal was obtained using a triboelectric nanogenerator (TENG), which runs in the vertical contact separation mode. A noiseless and amplified wrist pulse signal was produced by the active low pass filter and amplifier through Arduino Uno. The noise-free and amplified wrist pulse signal was displayed on a personal computer, as shown in Fig. 2.

Sensor fabrication

The TENG comprises two opposing charge layers that exchange charge upon contact or compression.[10] Fig. 3(A)

shows how the transferred charge generates a voltage across its output terminal. The structural design and operational principle of the TENG categorizes its four modes of operation into the single electrode, lateral sliding, vertical contact-separation, and freestanding triboelectric-layer types.[11] Among the four operating modes, the vertical contact-separation mode provides optimal output performance.[12,13] Consequently, the vertical contact-separation mode as employed by the TENG developed in this study. The vertical contact-separation mode is classified into two categories: dielectric-to-dielectric and conductor-to-dielectric models, based on the materials utilized in the dielectric pair of the TENG.[14] In comparison, the conductor-to-dielectric approach produces a superior output voltage. The conductor-to-dielectric model was employed to achieve optimal output from the proposed TENG.[15] The developed TENG is circular, with 12 mm in diameter and 350 μm in thickness. A commercially available Teflon tape together with conductive copper foil and aluminum foils were used in the design of the TENG. The Teflon tape (150 μm thickness) serves as the negative layer, with aluminum foil (24 μm thickness) functioning as the negative electrode, while the copper foil (70 μm thickness) acts as both the positive layer and positive electrode. The negative and positive layers were stacked together, and subsequently, the copper leads were linked to both
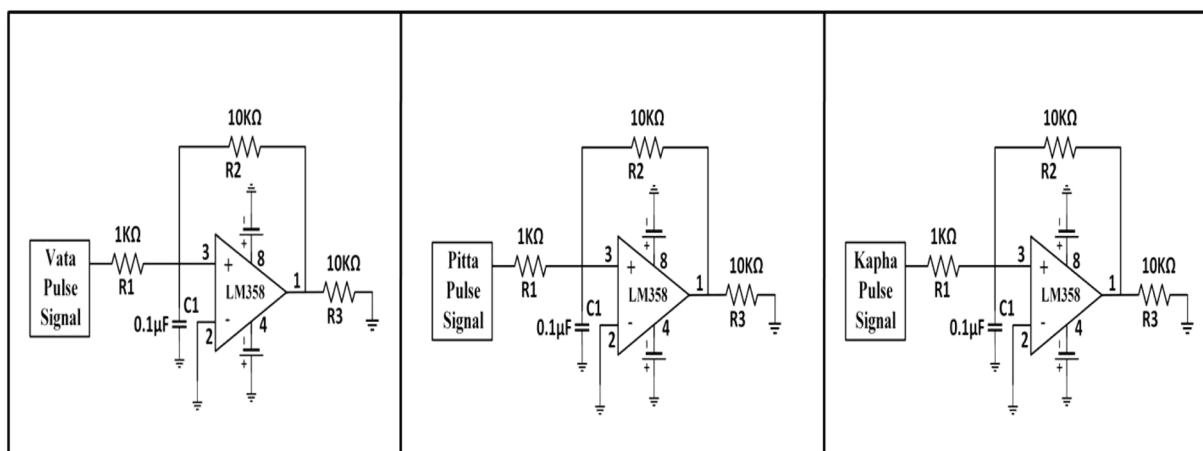

Fig. 4 Filter and amplifier circuit.

electrodes. The air gap between the positive and negative layers was ≈34 μm in thickness. Furthermore, a polypropylene film was employed to encapsulate the designed TENG to preserve its output performance under sweat and temperature conditions. The TENG was modeled in COMSOL Multiphysics as per the dimensions shown in Fig. 3(B) and subsequently simulated utilizing solid mechanics and electrostatics physics. In solid mechanics, the input pulse pressure is converted into displacement, while electrostatics utilizes the output displacement of solid mechanics as input and changes it into an electrical signal. The resultant electrical signal is exactly equal to the input pulse pressure imparted. Fig. 3(C) depicts the constructed model of the TENG for *nadi* signal collection. The negative layer, associated with its electrode, of the proposed TENG is situated at the *vata*, *pitta*, and *kapha* sites. *Vata*, *pitta*, and *kapha* each exert pressure that induces deformation in the negative layer, leading to contact between the positive and negative layers as long as the pressure is maintained. In the absence of *vata*, *pitta*, or *kapha* pressure, the two layers remain separate from each other. This contact and separation process generates charge transfers between the negative and positive layers. The assembled TENG is situated on the *vata nadi* location from which the signal is to be acquired, as illustrated in Fig. 3(D). The acquired *vata nadi* signal was displayed on a personal laptop. Similarly, the remaining two *nadi* signals were acquired by placing the fabricated TENG in their designated locations. Table 1 delineates the results of a comparative analysis of the pulse detecting device's materials, pressure sensitivity, and sensing range against other similar research. The designed TENG exhibits a high sensitivity of 41% kPa^{-1} throughout a pressure range of 0.01–3 kPa, with an exceptionally rapid response time of <3 ms. The sensitivity of the intended TENG is assessed by its open circuit voltage in response to the specified wrist pulse pressure (0–3 kPa). To achieve the highest output voltage from the proposed TENG, optimal materials and surface
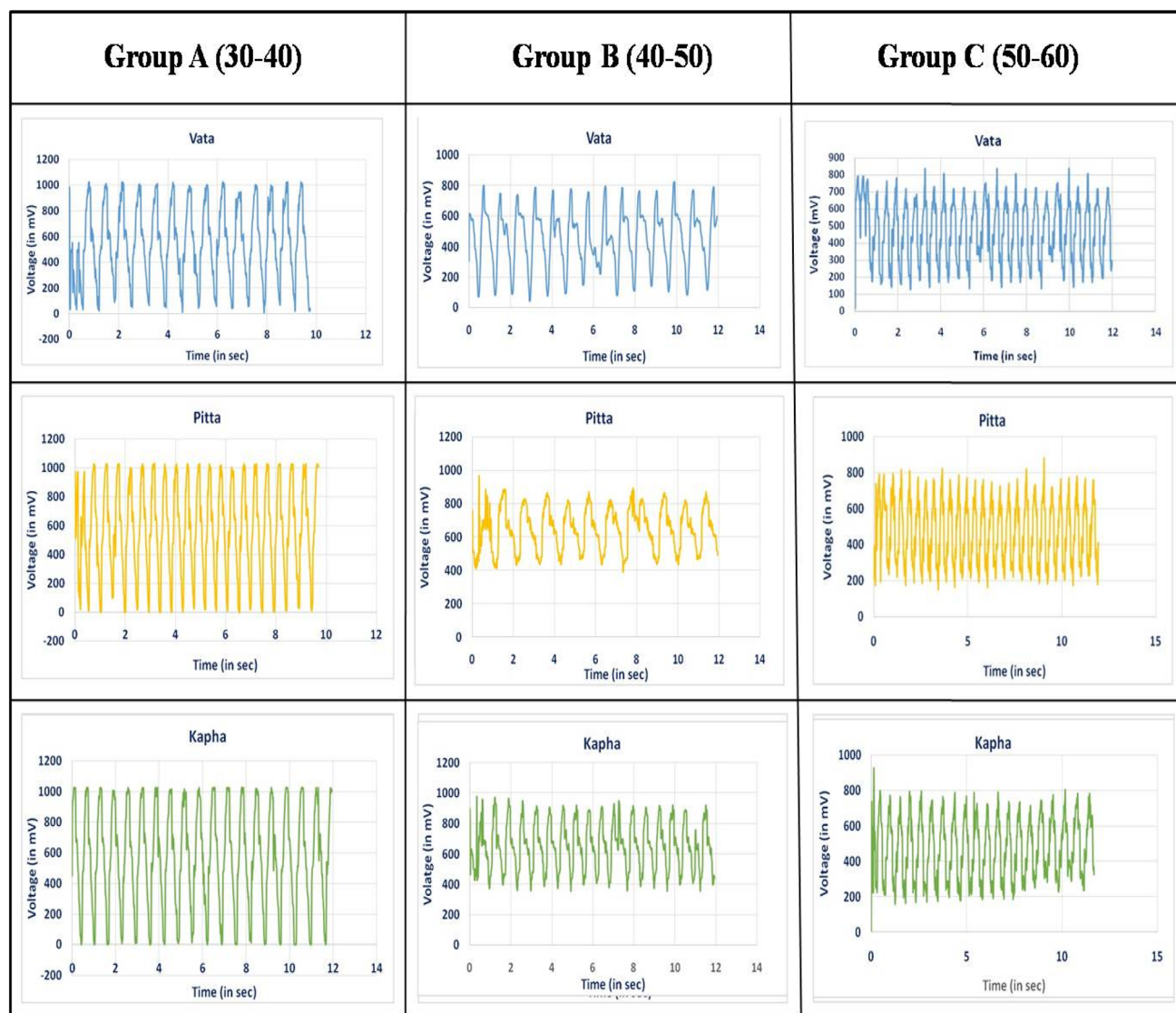

Fig. 5 Acquired *vata, pitta* and *kapha nadi* signals.

morphology were employed. The developed TENG, owing to its high sensitivity and sufficient sensing range, has the potential to capture the pulse signal.

Instrumentation setup

The three distinct TENGs were designed to be placed on the *vata*, *pitta*, and *kapha* locations of the human wrist (right for male and left for female) to harvest the three separate *nadi* signals. This study solely looks at the *vata nadi* because it is more likely to produce hypertension; nevertheless, the research also looks at the other *nadi* output signals.[21] The extracted *vata*, *pitta*, and *kapha nadi* signals exhibit low frequency ranges and noise.[6] An active low filter is recommended to remove any noise from the obtained three *nadi* signals. In this case, noise in the

three distinct *nadi* signals is eliminated using three independent active low-pass filters. For the intended low pass filter, the cutoff frequency is kept at 10 Hz. Fig. 4 shows the low-pass filters that were designed using the IC LM 358 amplifier. Although the operational amplifier's inverting input terminal is grounded, the obtained *nadi* signals are fed to the LM 358 operational amplifier's concerned non-inverting input terminal. Both noise reduction and signal amplification are achieved using the low-pass filter.

Analog input terminals A1, A2, and A3 of Arduino Uno are linked to the filtered *vata*, *pitta*, and *kapha nadi* signals to obtain the numerical values of the signals. Fig. 5 displays the plotted numerical data of the *vata*, *pitta*, and *kapha nadi* signals of a single subject of each group for 12 s. Through the internet of things (IoT), the physician receives the obtained numerical
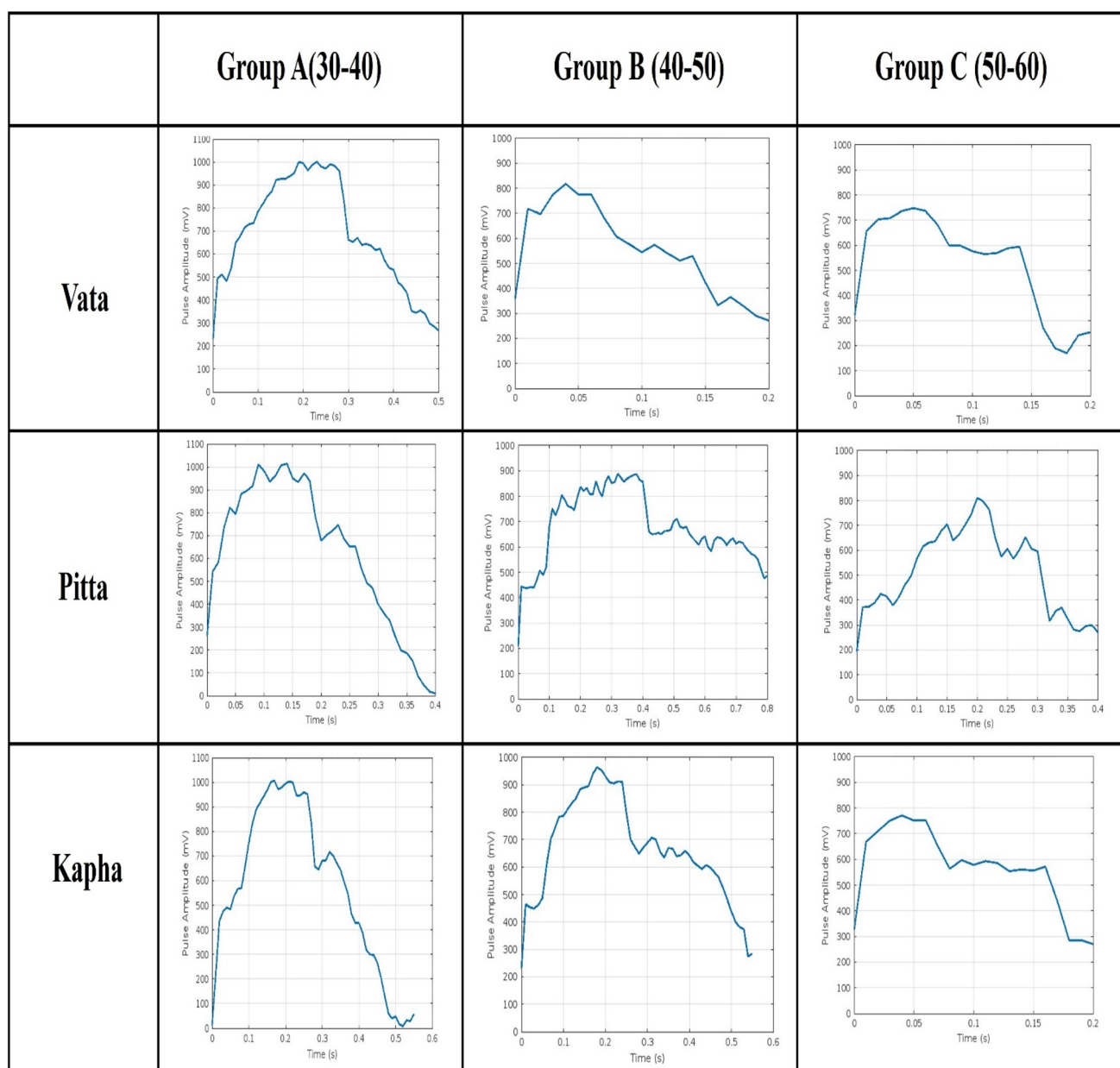

Fig. 6 Time domain analysis of the *vata, pitta* and *kapha nadi* signals.

values of the *vata*, *pitta*, and *kapha nadi* signals on their smartphone or computer.

Study subjects

The three *nadi* data collecting system involves a total of 100 healthy people (the study was carried out with the subjects' written consent). Initially, the subjects were requested to remain calm for 10 min to identify the location of the *vata*, *pitta* and *kapha nadi* signals on their wrist. To acquire these signals, the designed three distinct TENGs were placed on the *Vata*, *Pitta* and *Kapha nadi* signal locations of the subject's wrist. The three *nadi* signals were captured for 1 min; however, the obtained *nadi* signal contains noise and has insufficient amplitude. Separate active low-pass filters were designed for noise rejection and amplification. The filtered and amplified output of the three *nadi* signals were connected to an Arduino Uno analog input terminals through which we could observe the acquired three *nadi* signals or obtain numerical values of the acquired

three *nadi* signals. The above 100 subjects were categorized into three groups: group A subjects were in the age of 30–40 (16 male and 17 female), group B subjects were in the age of 40–50 (16 male and 17 female), and group C subjects were in the age of 50–60 (17 male and 17 female). Initially, the number of beats per minute for each subject was calculated from the acquired three *nadi* signals. Later, the frequency of *vata*, *pitta* and *kapha* for each subject were found. Next, the average frequency values for both genders in the above three groups were tabulated from 8 am to 8 pm.

Time domain analysis

The pulse amplitude, shape, and outlines were examined through the time domain analysis of the pulse signal. The time-domain characteristics of the pulse waveform typically include a percussive wave (P), tidal wave (T), valley (V), and dicrotic wave (D). The baseline serves as the measurement point for the aforementioned properties. However, as can be seen in Fig. 6,
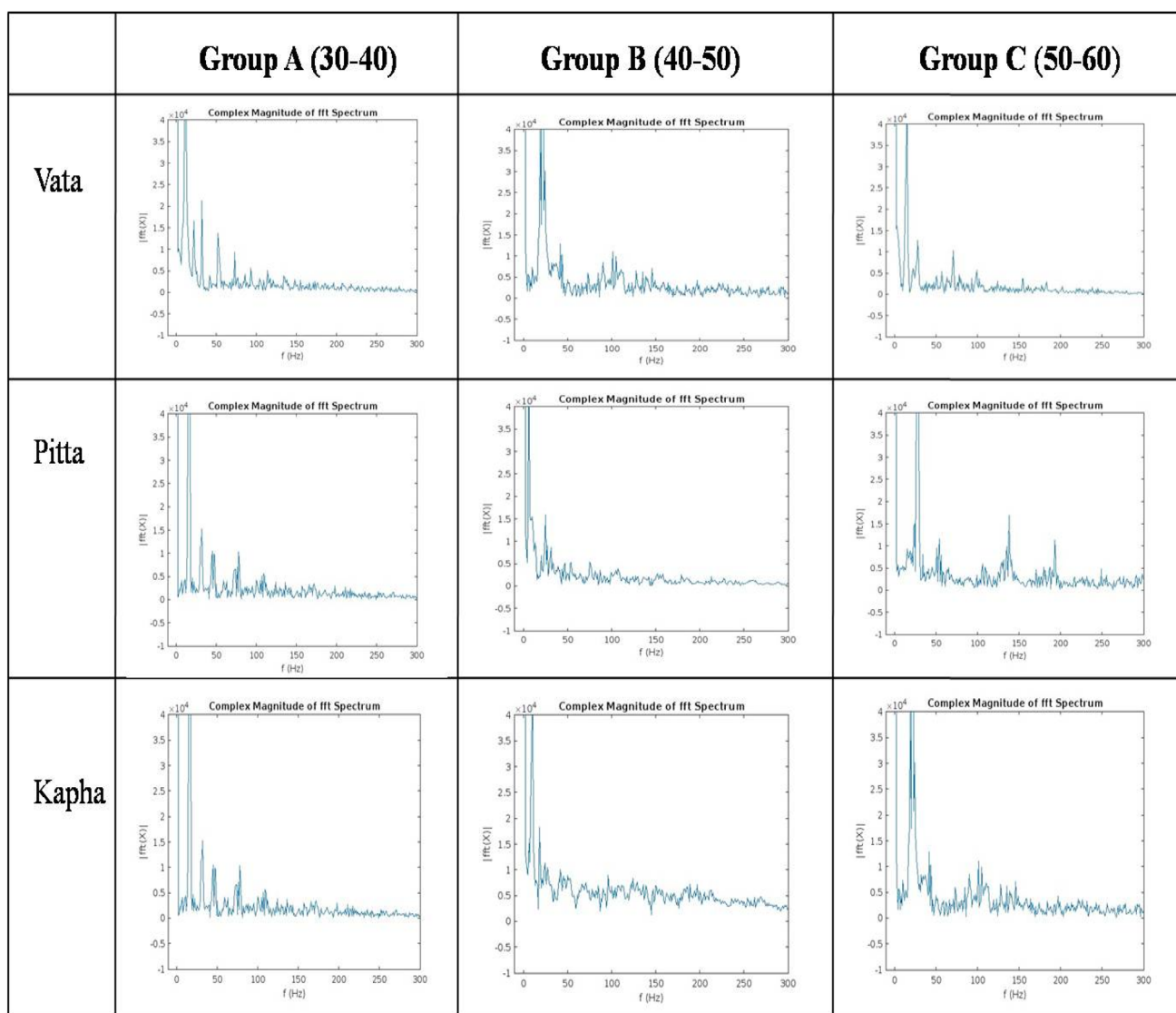

Fig. 7   Frequency domain of the *vata*, *pitta* and *kapha nadi* signals.

the groupwise three *nadi* pulse pressure is a result of the interaction of the tidal, percussion, and dicrotic waves. Groupwise, the pulse amplitude, shape and duration vary accordingly. Parameters such as the pulse peak amplitude, dicrotic notch, and pulse duration are considered while analyzing the health of the participants. The dicrotic and tidal waves have extremely small amplitudes in unwell people. Unlike the pulse shape of the healthy subjects, that of sick subjects varies more with an increasing static pressure.

Frequency domain analysis

The pulse resonance frequency, pulse energy, and pulse power spectrum were examined using the frequency domain study of pulse signals. Every organ in the human body has a resonance frequency of its own, and the information about its physiological state and pathology can be found in its harmonics. Herein,

the dominant harmonic frequency of the acquired *vata*, *pitta*, and *kapha nadi* signals of a single subject of each group was analyzed using the fast Fourier transform, as illustrated in Fig. 7. It is observed that in all the three groups, the highest harmonics frequency on the three *nadi* signals exist within 0–40 Hz. This harmonic frequency variation decides the stiffness of the vessel. The highest power distribution of the obtained *vata*, *pitta*, and *kapha nadi* signals was found using the Welch's power spectral density estimation, as depicted in Fig. 8.

Results and discussion

In Ayurveda, the diagnosis of BP relies on the shape, size, duration, and amplitude of the *nadi* pulse. This study considered three distinct healthy people within a specified age category from whom *vata*, *pitta*, and *kapha nadi* pulse signals were gathered. The time domain analysis yields the shape, size,
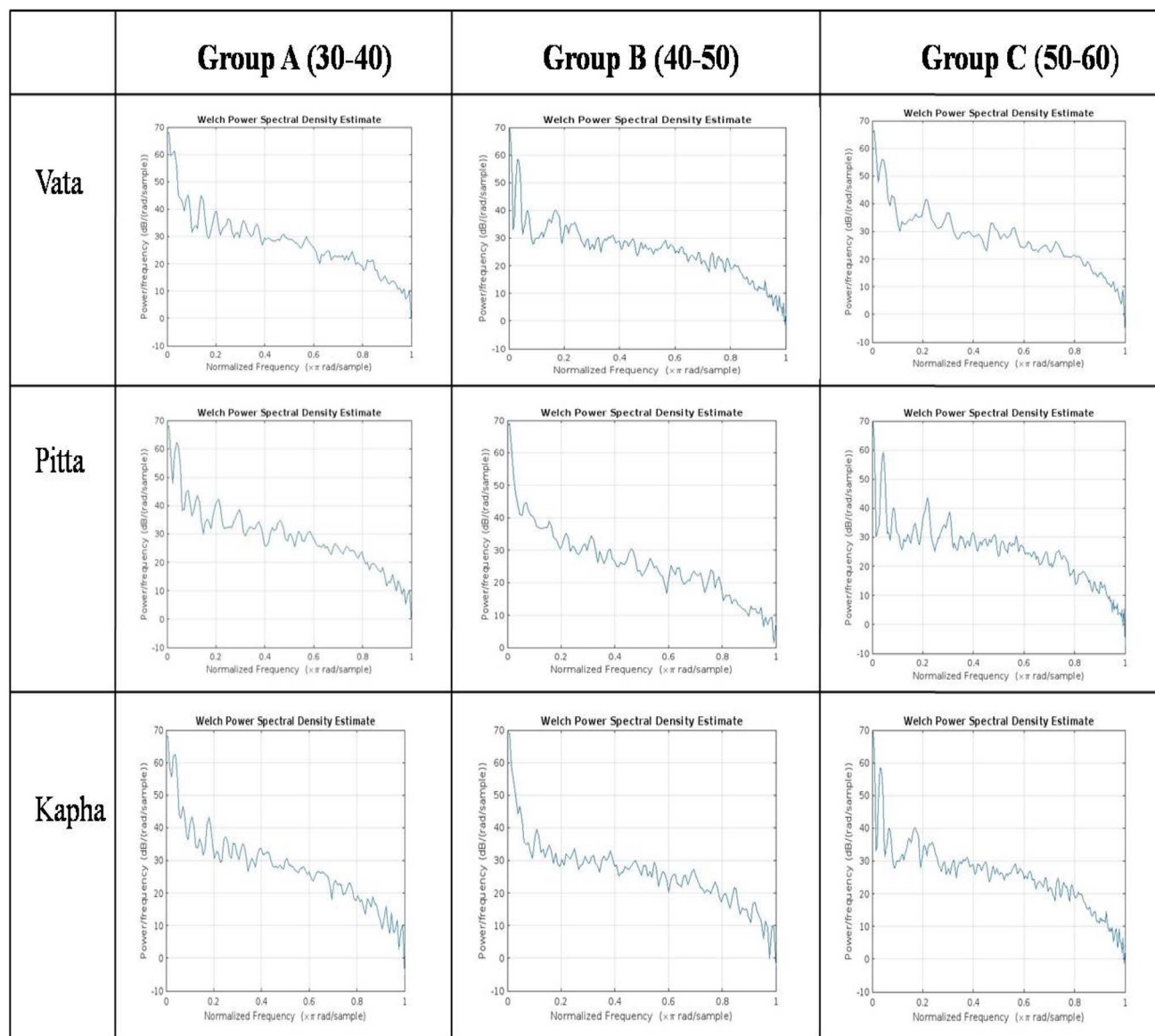

Fig. 8   Power spectral density estimate of the *vata, pitta* and *kapha nadi* signals.

duration, and amplitude of the collected *vata*, *pitta*, and *kapha nadi* pulses.

The acquired *vata*, *pitta*, and *kapha nadi* pulses of all the three groups were characterized using a percussive wave (P), tidal wave (T), valley (V), and dicrotic wave (D). It is evident that the acquired *vata*, *pitta*, and *kapha nadi* pulses have a dissimilar morphology among the three groups owing to the age difference.

A normal *vata nadi* pulse takes 0.5 s and 1000 mV in group A, 0.2 s and 800 mV in group B, and <0.2 s and >700 mV in group C. This implies that the beats per minute of group C-aged subjects are more than those of group B-aged subjects, whereas the beats per minute of group B-aged subjects are more than those of group A. These variations in beats per minute among the three age groups are also caused by age differences. This work will assist Ayurvedic doctors to determine a person's BP and other illnesses if they are in the age categories outlined above using these data as a standard or reference. Table 2 shows the amplitude of the signals mentioned. The amplitude of *vata*, *pitta* and *kapha* will vary on a case-by-case basis. Accordingly,

the harmonic frequency and power distribution also varies. Fig. 9(A–C) illustrates the bar chart for the amplitude, harmonic frequency and power spectral density estimates of the acquired *vata*, *pitta* and *kapha nadi* signals.

Through frequency domain analysis, the dominant harmonic frequency and maximum power distribution of the acquired *vata*, pitta and *kapha nadi* signals were found; they are listed in Tables 3 and 4.

The three *nadi* signal frequencies of the male and female subjects are dissimilar.[22] The *vata nadi* frequencies of male

Table 3 Harmonic frequency of the acquired *vata*, *pitta* and *kapha nadi* signals

	Group A	Group B	Group C
Vata	0–20 Hz	0–40 Hz	0–20 Hz
Pitta	0–20 Hz	0–10 Hz	0–40 Hz
Kapha	0–20 Hz	0–10 Hz	0–40 Hz

Table 4 Maximum power distribution of the acquired *vata*, *pitta* and *kapha nadi* signals

	Group A	Group B	Group C
Vata	68 dB	69 dB	68 dB
Pitta	68 dB	69 dB	70 dB
Kapha	68 dB	69 dB	70 dB

Table 2 Amplitude of the acquired *vata*, *pitta* and *kapha nadi* signals

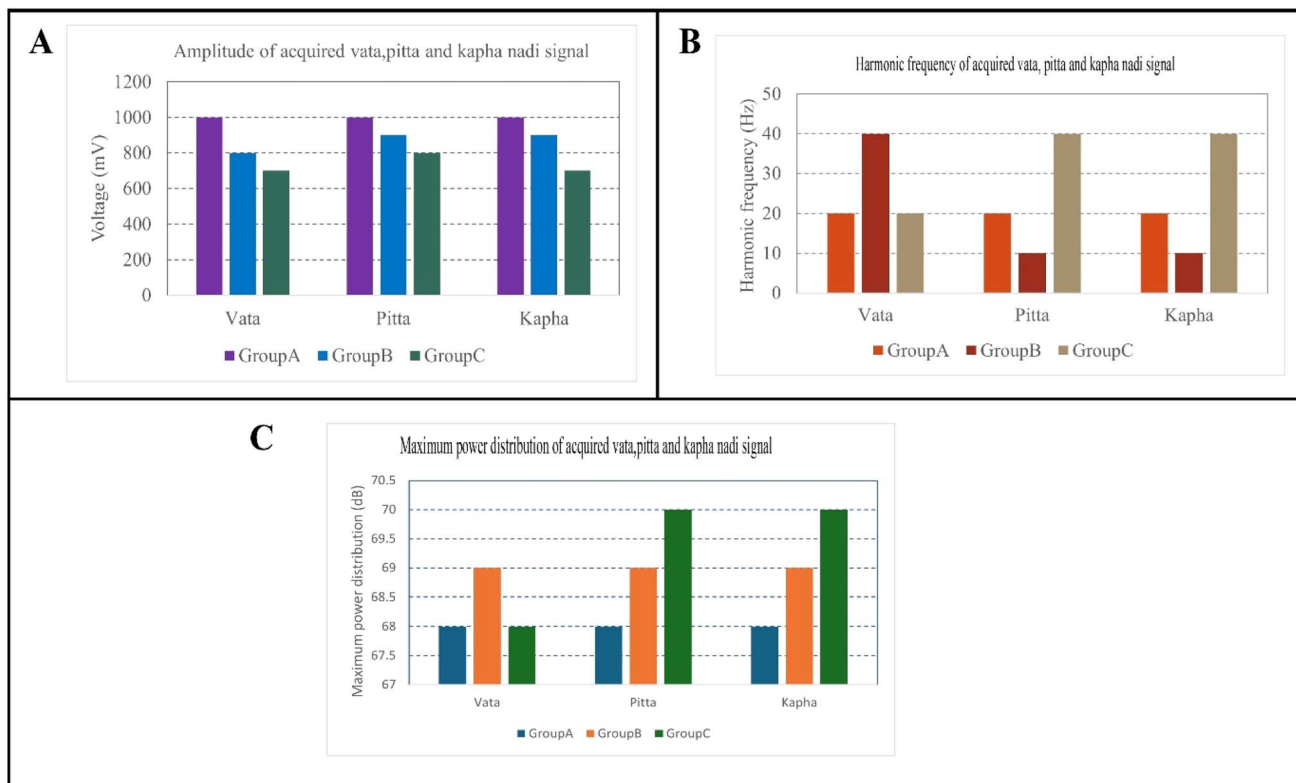|	Group A	Group B	Group C
Vata	1000 mV	800 mV	>700 mV
Pitta	1000 mV	900 mV	800 mV
Kapha	1000 mV	>900 mV	>700 mV

Fig. 9 (A) Amplitude bar chart of the acquired *vata*, *pitta* and *kapha nadi* signals. (B) Harmonic frequency bar chart of the acquired *vata*, *pitta* and *kapha nadi* signals. (C) Power spectral density estimate bar chart of the *vata*, *pitta* and *kapha nadi* signals.

Table 5 Frequency range of the three *nadi* signals

Age	Gender	Nadi	8 am	10 am	12 pm	2 pm	4 pm	6 pm	8 pm
30–40	Male	Vata	1.51 Hz	1.50 Hz	1.48 Hz	1.42 Hz	1.30 Hz	1.31 Hz	1.33 Hz
		Pitta	1.30 Hz	1.28 Hz	1.27 Hz	1.23 Hz	1.10 Hz	1.15 Hz	1.16 Hz
		Kapha	1.19 Hz	1.16 Hz	1.07 Hz	0.97 Hz	0.82 Hz	1.07 Hz	0.83 Hz
	Female	Vata	1.53 Hz	1.51 Hz	1.49 Hz	1.43 Hz	1.32 Hz	1.32 Hz	1.34 Hz
		Pitta	1.30 Hz	1.29 Hz	1.27 Hz	1.23 Hz	1.10 Hz	1.52 Hz	1.28 Hz
		Kapha	1.17 Hz	1.10 Hz	1.00 Hz	0.93 Hz	0.87 Hz	1.03 Hz	0.81 Hz
40–50	Male	Vata	1.53 Hz	1.51 Hz	1.46 Hz	1.35 Hz	1.32 Hz	1.42 Hz	1.34 Hz
		Pitta	1.32 Hz	1.21 Hz	1.37 Hz	1.21 Hz	1.12 Hz	1.10 Hz	1.12 Hz
		Kapha	1.20 Hz	1.06 Hz	1.15 Hz	1.07 Hz	0.98 Hz	1.00 Hz	0.79 Hz
	Female	Vata	1.55 Hz	1.53 Hz	1.39 Hz	1.38 Hz	1.41 Hz	1.33 Hz	1.41 Hz
		Pitta	1.29 Hz	1.31 Hz	1.29 Hz	1.21 Hz	1.19 Hz	1.09 Hz	1.15 Hz
		Kapha	1.21 Hz	1.05 Hz	1.22 Hz	0.98 Hz	0.91 Hz	0.89 Hz	0.82 Hz
50–60	Male	Vata	1.59 Hz	1.58 Hz	1.42 Hz	1.41 Hz	1.39 Hz	1.29 Hz	1.38 Hz
		Pitta	1.22 Hz	1.34 Hz	1.19 Hz	1.24 Hz	1.13 Hz	1.11 Hz	1.14 Hz
		Kapha	1.19 Hz	1.12 Hz	1.01 Hz	0.92 Hz	0.86 Hz	0.79 Hz	0.83 Hz
	Female	Vata	1.58 Hz	1.55 Hz	1.47 Hz	1.43 Hz	1.38 Hz	1.32 Hz	1.34 Hz
		Pitta	1.33 Hz	1.31 Hz	1.19 Hz	1.25 Hz	1.19 Hz	1.20 Hz	1.16 Hz
		Kapha	1.21 Hz	1.15 Hz	0.97 Hz	1.19 Hz	0.93 Hz	1.01 Hz	0.75 Hz

subjects from the above three groups were around 1.59–1.29 Hz. Similarly, female subjects' *vata nadi* frequencies were around 1.58–1.32 Hz. The *pitta nadi* frequencies of male subjects from the above three groups were around 1.34–1.10 Hz. Similarly, female subjects' *pitta nadi* frequencies were around 1.33–1.10 Hz. The *kapha nadi* frequencies of male subjects from the above three groups were around 1.21–0.75 Hz. Similarly, female subject's *kapha nadi* frequencies were around 1.22–0.75 Hz. The frequency range of the three *nadi* signals of male and female subjects belonging to the three different groups are tabulated in Table 5.

Conclusion

The designed TENG has potential to acquire the three *nadi* signals of three distinct groups, which are necessary for diagnosing BP-related illnesses. In this study, three distinct groups of healthy subjects were examined and their three *nadi* signals were acquired. The time and frequency domains of the acquired three *nadi* signals were analyzed. An Ayurvedic doctor can use these data as a reference to determine patients' BP and other ailments if the patients fall into the above-mentioned groups. Moreover, three distinct groups of male and female participants had their *nadi* pulses taken, and their frequencies were calculated. The attributes of the developed TENG include affordability, lightweight, reusability, and ease of operation. Furthermore, the relative humidity during testing has no effect on the intended TENG output performance. The reported TENG is only suitable for medical monitors owing to its size restriction.

Ethical statement

Ethics approving committee: Institutional Ethical Committee for Studies on Human Subjects. Ethics approval number: VIT/IECH/XIII/2023/04. Ethics approval date: 31.03.2023. To carry out this study, written consent from the subjects was collected, and no minor was involved in this study.

Data availability

Data are available from the corresponding author upon request.

Author contributions

Karthikeyan V: conceived and designed the experiments; performed the experiments; analyzed and interpreted the data; contributed materials, analysis tools and data; and wrote the paper. Vivekanandan S: conceived and designed the experiments; analyzed and interpreted the data; and contributed materials, analysis tools and data.

Conflicts of interest

On behalf of all authors, the corresponding author states that there is no conflict of interest.

References

1 A. A. Mathew, A. Chandrasekhar and S. Vivekanandan, A review on real-time implantable and wearable health monitoring sensors based on triboelectric nanogenerator approach, *Nano Energy*, 2021, **80**(2020), 105566, DOI: **10.1016/j.nanoen.2020.105566**.

2 H. Ouyang, et al., Self-Powered Pulse Sensor for Antidiastole of Cardiovascular Disease, *Adv. Mater.*, 2017, **29**(40), 1–10, DOI: **10.1002/adma.201703456**.

3 A. Chandrasekhar, N. R. Alluri, B. Saravanakumar, S. Selvarajan and S. J. Kim, Human Interactive Triboelectric Nanogenerator as a Self-Powered Smart Seat, *ACS Appl. Mater. Interfaces*, 2016, **8**(15), 9692–9699, DOI: **10.1021/acsami.6b00548**.

4 V. Karthikeyan and S. Vivekanandan, Optimize an effective triboelectric nanogenerator surface morphology to harvest the human wrist pulse pressure: A numerical study on finite element method, *Heliyon*, 2022, **8**(12), e12109, DOI: **10.1016/j.heliyon.2022.e12109**.

5 J. K. Mainra, A. Kaur, G. Sapra and P. Gaur, Simulation and Modelling of Triboelectric Nanogenerator for Self-powered Electronic Devices, *IOP Conf. Ser. Mater. Sci. Eng.*, 2022, **1225**(1), 012012, DOI: **10.1088/1757-899x/1225/1/012012**.

6 A. A. Mathew and S. Vivekanandan, A review on ayurvedic approach in sphygmology: Characteristics, traditional parameters and existing sensors in sphygmology, *Int. J. Sci. Technol. Res.*, 2020, **9**(3), 7188–7204.

7 D. Zhang, W. Zuo, D. Zhang, H. Zhang and N. Li, Wrist blood flow signal-based computerized pulse diagnosis using spatial and spectrum features, *J. Biomed. Sci. Eng.*, 2010, **3**, 361–366, DOI: **10.4236/jbise.2010.34050**.

8 H. Chang, J. Chen and Y. Liu, ScienceDirect Micro-piezoelectric pulse diagnoser and frequency domain analysis of human pulse signals, *J. Tradit. Chin. Med. Sci.*, 2018, **5**(1), 35–42, DOI: **10.1016/j.jtcms.2018.02.002**.

9 Y. K. Yim, C. Lee, H. J. Lee and K. S. Park, Gender and Measuring-position Differences in the Radial Pulse of Healthy Individuals, *J. Acupunct. Meridian Stud.*, 2014, **7**(6), 324–330, DOI: **10.1016/j.jams.2014.06.014**.

10 A. A. Mathew and V. Shanmugasundaram, Fabrication of Screen-Printed Single-Electrode Triboelectric Nanogenerator-Based Self-Powered Sensor for Pulse Measurement and Its Characterization, *Energy Technol.*, 2023, **11**(7), 1–15, DOI: **10.1002/ente.202300174**.

11 H. Feng, C. Zhao, P. Tan, R. Liu, X. Chen and Z. Li, Nanogenerator for Biomedical Applications, *Adv. Healthcare Mater.*, 2018, **7**(10), 1–18, DOI: **10.1002/adhm.201701298**.

12 M. Ma, *et al.*, Development, applications, and future directions of triboelectric nanogenerators, *Nano Res.*, 2018, **11**(6), 2951–2969, DOI: **10.1007/s12274-018-1997-9**.

13 A. A. Mathew and S. Vivekanandan, Design and Simulation of Single-Electrode Mode Triboelectric Nanogenerator-Based Pulse Sensor for Healthcare Applications Using COMSOL Multiphysics, *Energy Technol.*, 2022, **2101130**, 1–12, DOI: **10.1002/ente.202101130**.

14 H. Chen, Y. Xu, J. Zhang, W. Wu and G. Song, Theoretical System of Contact-Mode Triboelectric Nanogenerators for High Energy Conversion Efficiency, *Nanoscale Res. Lett.*, 2018, **13**(1), 346, DOI: **10.1186/s11671-018-2764-2**.

15 G. R. Chen, Y. F. Huang, Y. Y. Chen, C. Y. Wu and Y. C. Tsai, A flexible triboelectric nanogenerator integrated with an artificial petal micro/nanostructure surface, *Jpn. J. Appl. Phys.*, 2019, **58**, SDDL02, DOI: **10.7567/1347-4065/ab0de9**.

16 J. Liang, Z. Zhao, Y. Tang, X. Hao, X. Wang and J. Qiu, Covalent bonds-integrated graphene foam with superb electromechanical properties as elastic conductor and compressive sensor, *Carbon*, 2019, **147**, 206–213, DOI: **10.1016/j.carbon.2019.02.087**.

17 X. Dong, Y. Wei, S. Chen, Y. Lin, L. Liu and J. Li, A linear and large-range pressure sensor based on a graphene/silver nanowires nanobiocomposites network and a hierarchical structural sponge, *Compos. Sci. Technol.*, 2018, **155**, 108–116, DOI: **10.1016/j.compscitech.2017.11.028**.

18 S. Wang, Z. Zhang, Z. Chen, D. Mei and Y. Wang, Development of Pressure Sensor Based Wearable Pulse Detection Device for Radial Pulse Monitoring, *Micromachines*, 2022, **13**(10), 1699, DOI: **10.3390/mi13101699**.

19 Z. Chen, Z. Wang, X. Li, Y. Lin, N. Luo, M. Long, N. Zhao and J.-B. Xu, Flexible Piezoelectric-Induced Pressure Sensors for Static Measurements Based on Nanowires/Graphene Heterostructures, *ACS Nano*, 2017, **11**(5), 4507–4513, DOI: **10.1021/acsnano.6b08027**.

20 S. Sharma, A. Chhetry, H. Yoon and J. Y. Park, Wearable Capacitive Pressure Sensor Based on MXene Composite Nano fi brous Scaffolds for Reliable Human Physiological Signal Acquisition, *ACS Appl. Mater. Interfaces*, 2020, **12**(19), 22212–22224, DOI: **10.1021/acsami.0c05819**.

21 M. Menon and A. Shukla, Journal of Ayurveda and Integrative Medicine Understanding hypertension in the light of Ayurveda, *J. Ayurveda Integr. Med.*, 2017, 1–6, DOI: **10.1016/j.jaim.2017.10.004**.

22 K. Basavaraj and S. Balaji, Nadi Pariksha: A Novel Machine Learning Based Wrist Pulse Analysis through Pulse Auscultation System using K-NN Classifier, *Int. J. Electron. Commun. Eng. Technol.*, 2021, **12**(3), 1–10, DOI: **10.34218/IJECET.12.3.2021.001**.